Transient Analysis of Microgrids with Parallel Synchronous Generators and Virtual Synchronous Generators

Shi, Kai; Song, Wentao; Ge, Huilin; Xu, Peifeng; Yang, Y.; Blaabjerg, F.

Published in:
IEEE Transactions on Energy Conversion

DOI (link to publication from Publisher):
10.1109/TEC.2019.2943888

Publication date:
2020

Document Version
Accepted author manuscript, peer reviewed version

Transient Analysis of Microgrids with Parallel Synchronous Generators and Virtual Synchronous Generators

Kai Shi, Wentao Song, Huilin Ge, Peifeng Xu, Yongheng Yang, *Senior Member, IEEE*, and Frede Blaabjerg, *Fellow, IEEE*

***Abstract*—In recent years, the increasing penetration of distributed generation in microgrids challenges the control and coordination of energy resources. Especially in microgrids with virtual synchronous generator (VSG)-controlled converters and conventional synchronous generators (SG), the inherent inertia difference (i.e., the VSG and SG) results in a poor transient performance when the VSG and/or loads are cut in/out. Thus, this paper explores the transient performance of microgrids with parallel VSG and SG systems. More importantly, a novel pre-synchronization control method is proposed to eliminate the phase jump while meeting the requirements in case of closures or re-closures of generation units. A small-signal dynamic model is presented, and accordingly, the VSG inertia and its damping can be designed considering the capacity ratio of VSG and SG units. In addition, with the power angle stability analysis, an active power provision strategy is introduced to suppress the transient power oscillation due to the inertia difference. Finally, the feasibility of the proposed methods is verified by simulations on a microgrid consisting of parallel VSG and SG units.**

***Index Terms*-Microgrid, virtual synchronous generator (VSG), synchronous generator (SG), power oscillation, stability, inertia matching, transient performance; pre-synchronization**

I. Introduction

With the fast development of the distributed generation (DG) technology, the capacity ratio of conventional synchronous generators (SG) decreases gradually in recent years in microgrid applications. On the other hand, the DG units can be controlled by the virtual synchronous generator (VSG) method to mimic an SG, which improves the stability of the entire power system [1]. Thus, many attempts have been made to advance the VSG technology, typically considering the inertia and damping characteristics [2], [3], stability issues [4], [5], operational modes (islanded and grid-connected) [6] and general control strategies [7].

In a remote microgrid where the main grid is not available, the small schedulable SG units are usually used as the main power supply and the renewable-based DG units are used as the secondary supply. Due to the inherent difference in inertia and capacity between the SG and DG, the entire system dynamics vary significantly. Changes in power supply or load often occur in such a microgrid, and an important index of its stability and reliability is whether it can provide sufficient frequency support during a frequency dip. Consequently, the focus has been put on the control and coordination of various generators [8].

To address the parallel operation stability issues of DGs during transient operation, a virtual impedance concept and a VSG model with optimized inertia and damping were implemented to avoid frequency and power oscillations [9]-[12]. However, it is known that the focus in the literature was on the operation of parallel VSGs. When SGs are cut in, the system stability may be challenged due to the difference of the moment of inertia and prime mover shaft inertia for the VSG and SG units. In this case, the VSG-controlled units respond with fast dynamics to system disturbances, e.g., energy sources cutting-in/out and load changes, which may induce severe transient power oscillations. Consequently, the oscillations affect the conventional SG rotor speed and lower the capacity of power allocations among units. The system may eventually go into instability.

Unfortunately, the mechanism of the instability for parallel SG and VSG units has not been clearly revealed. In [13] and [14], the inertia difference between inverters and SGs was analyzed, where the frequency oscillation and poor transient power sharing were discussed. Moreover, the VSG control system was introduced to achieve better inertia response characteristic. Nevertheless, the system model and parameters were not unified, and thus, transient instability issues may appear, even when the system is stable in steady state. In [15], a specific configuration of VSGs was proposed to improve the transient performance under load variations, while the capacity ratio of VSGs and SGs was not considered. In [16], the operation conditions were extended to unbalanced loading, and the transient virtual impedance was added to VSGs to alleviate the SG rotor speed deviation. It can be seen that the difference in response speed caused the instability of the voltage at the point of common-coupling (PCC), which led to high-frequency oscillations of output power. Moreover, although the dynamic performance is improved, the cutting-in characteristics are not considered in the parallel operation of VSGs and SGs.

Additionally, if the parallel operation pre-synchronization algorithm is not properly designed, poor transients may occur during the closure of circuit breakers [17]. In the prior-art

This work is supported by the National Natural Science Foundation of China under grant 51407085, In part by Natural Science Research Projects of Jiangsu Higher Education Institutions under grant 18KJD470004, In part by National Key R&D Program of China under grant 2017YFB0103200 and in part by the Project Funded by the Priority Academic Program Development of Jiangsu Higher Education Institution.

K. Shi, W. Song, and P. Xu are with the School of Electrical and Information Engineering, Jiangsu University, Zhenjiang, 212013, China.

H. Ge is with the College of Electricity and Information, Jiangsu University of Science and Technology, Zhenjiang, 212013, China.

Y. Yang and F. Blaabjerg are with the Department of Energy Technology, Aalborg University, Aalborg East 9220, Denmark.

Corresponding author: Peifeng Xu, E-mail: xupeifeng2003@126.com.

The final version of record is available at http://dx.doi.org/10.1109/TEC.2019.2943888

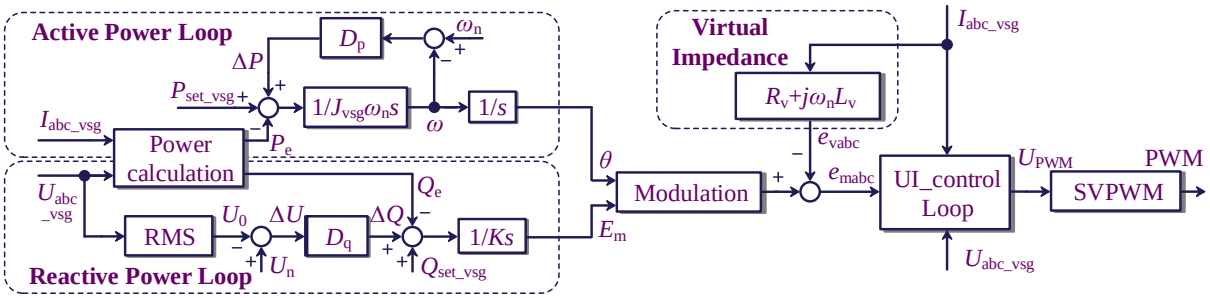

Fig. 1. General control block diagram of the virtual synchronous generation (VSG) technology (RMS – Root Mean Square; PWM – Pulse Width Modulation; SVPWM – Space Vector Pulse Width Modulation).

research, the pre-synchronization has been relatively matured, while phase errors should be further alleviated. For instance, a self-synchronization method of the grid-connected inverter based on the virtual impedance was proposed in [18]. The paper provided ideas for the VSG pre-synchronization but the LC filter impact was not considered. In turn, voltage phase deviations appear. In [19], a VSG pre-synchronization unit based on the virtual power and secondary control was proposed, where the frequency and voltage amplitude were realized by a secondary controller. However, in this case, the phase synchronization must be performed after the secondary control and the regulation signal is irregular. In [20], [21], the phase difference was added to the frequency control loop through a proportional-integral (PI) regulator to improve the phase synchronization. However, the periodic phase jump may lead to slow dynamics, or even synchronization failures, which will be further elaborated in Section III in this paper.

In light of the above, an enhanced pre-synchronization control method is proposed to eliminate the phase angle jump impact on the transient electromagnetic performance of microgrids. Then, the VSG parameter design and power provision mode are analyzed considering the inertia matching based on the small-signal model. The rest of this paper is organized as follows. In Section II, the basics of the VSG and SG control are introduced with the description of the parallel system. The proposed parallel pre-synchronization method is presented in Section III, and then, the small-signal model and the power allocation mode are discussed in Section IV. To verify the effectiveness of the proposed methods, simulations are performed, and the results are presented in Section V. Finally, Section VI concludes this paper.

II. Basic Principle and Mathematical Model

A. Basics of the VSG Technology

The general control block diagram of the VSG is shown in Fig. 1, where the active and reactive power loops emulate the rotor motion with the prime mover and the excitation controller of a conventional SG, respectively. Thus, the VSG can provide the entire modulation signal for the system [22]. Additionally, the output three-phase current of the inverter is added to the virtual impedance module and the three-phase synthetic voltage of the VSG minus the virtual voltage drop e_{vabc} [23], as shown in Fig. 1. Then, the output voltage e_{mabc} is modulated by the voltage and current double-loop control, and at last, the driving signals to power converter can be obtained through the space vector modulation (SVPWM).

According to the system shown in Fig. 1, the VSG system can be described as [24]

$$\begin{cases} P_{set\_vsg} + D_p(\omega_n - \omega) - P_e = J_{vsg}\omega_n \dfrac{d\omega}{dt} \\ Q_{set\_vsg} + D_q(U_n - U_0) - Q_e = K\dfrac{dE_m}{dt} \\ \delta = \int(\omega - \omega_n)dt \end{cases} \tag{1}$$

where P_{set_vsg} and Q_{set_vsg} are the given active and reactive power, D_p and D_q are the coefficients of the active power-frequency (P-ω) and reactive power-voltage (Q-V) droop relationships, P_e and Q_e are the electromagnetic power, J_{vsg} and K are the virtual moment of inertia and voltage coefficient, respectively, ω_n and ω are the rated and actual rotor angular frequency, U_n and U_0 are the effective values of the rated and actual voltage amplitude, E_m is the internal potential amplitude of the VSG, and δ is the power angle.

B. Control System Model of the SG

An SG control system, which is a feedback control to regulate the output frequency, voltage and power [16], is shown in Fig. 2. It consists of a governor (GOV) and an automatic voltage regulator (AVR). The GOV adjusts the prime mover shaft power P_{m_sg} according to the SG output angular frequency ω_{sg} and the rated angular frequency ω_n, in which k_p is the GOV proportional coefficient. The inherent large inertia brings a response delay to the shaft power, which results in power mismatching instantaneously after load mutation. Moreover, the rotor kinetic energy of an SG is consumed to compensate for the power shortage, which leads to the deviation of the angular frequency. Consequently, the

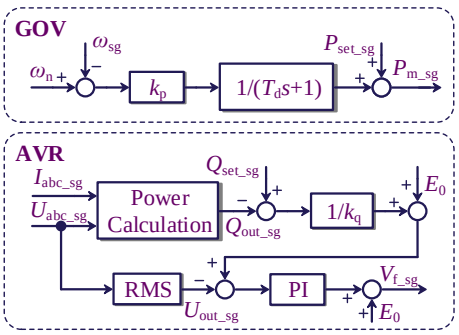

Fig. 2. Control diagram of the governor (GOV) and the automatic voltage regulator (AVR), where PI represents a proportional integral controller.

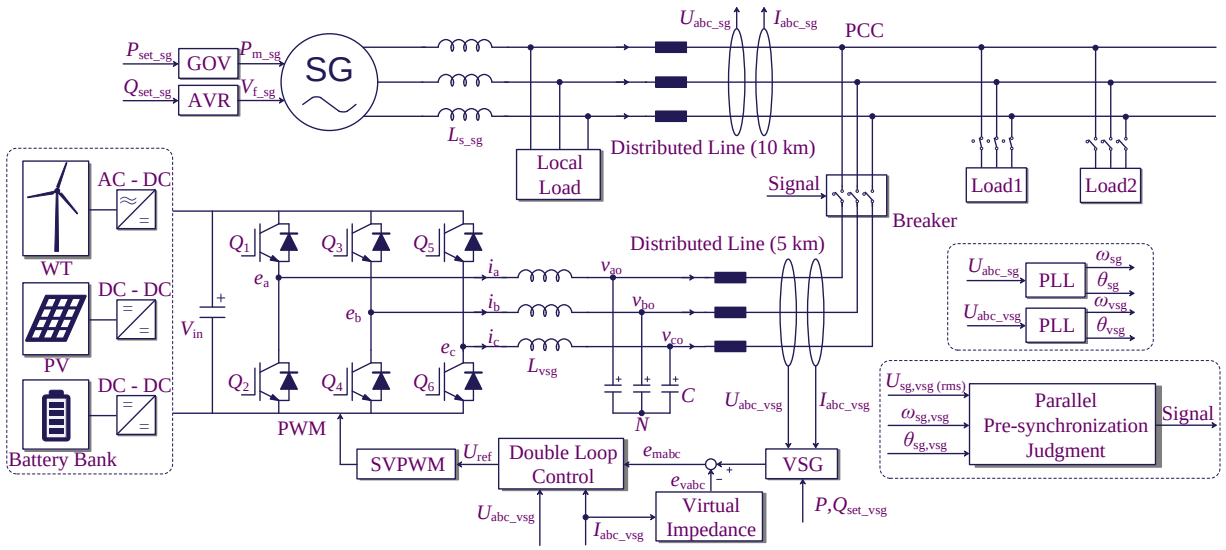

Fig. 3. System structure of a microgrid with parallel VSG and SG units, where the VSG can be fed by renewable energy sources (e.g., wind turbines – WT, photovoltaics – PV, and battery banks). Here, PLL represents the phase locked loop and PCC is the point of common-coupling.

system may become unstable. As it is shown in Fig. 2, a first-order inertial link, i.e., $1/(T_d s+1)$, is added into the GOV control loop to emulate the response delay of the mechanical system, where T_d is the governor inertial response time constant.

As the excitation system of an SG, the AVR consists of the excitation regulator and power unit, which is demonstrated in Fig. 2. The excitation regulator provides the DC excitation current to indirectly regulate the SG field voltage V_{f_sg}, and the employed excitation power unit ensures the reactive power allocation, as shown in Fig. 2, in which k_q is the AVR droop coefficient. Here, a PI controller has been employed as the output field voltage regulator.

C. Microgrids with Parallel VSG and SG Units

In this paper, in order to study the coordination of different generation resources in microgrids, an SG driven by a prime motor is selected as the main power supply. The above control scheme is adopted. A power inverter-fed system is connected in parallel with the SG, which is controlled through the VSG technology discussed in Section II.A. Clearly, as it is shown in Fig. 3, when the breaker is open, the SG is operating, and solely supplying the loads. In this case, the VSG system is discussed and disabled. In contrast, when the breaker is closed, the SG and the VSG should share the loading power properly to maintain the entire system stability. However, as discussed in previous sections, the microgrid may go into instabilities in the case of transient eventualities (e.g., sudden load/power source changes that may happen in renewable energy-based systems).

III. Pre-synchronization Algorithm

A. Analysis of Phase Angle Difference Jump

In order to reduce the electromagnetic and mechanical impact and ensure the smooth cutting-in of the VSG system in microgrids governed by an SG, the instantaneous output voltage of the VSG and SG should be consistent and have the same tendency, including amplitude, frequency and phase

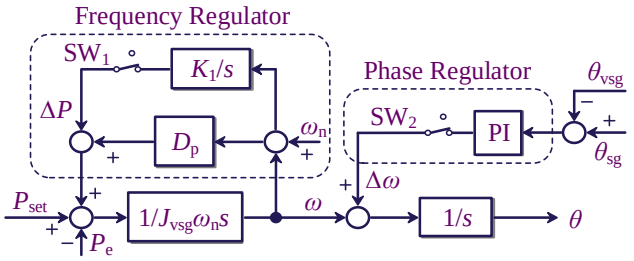

Fig. 4. Traditional VSG pre-synchronization algorithm.

before transients [19]. Thus, the pre-synchronization is of high concern to ensure stable operation, especially in the system with weak overloading capacity.

The VSG pre-synchronization is like the synchronization in grid-connected applications (typically, a phase-locked loop is adopted for synchronization). As exemplified in Fig. 4, an integral regulator (i.e., K_1/s) is applied to adjust the frequency difference, so does the voltage amplitude difference, which is relatively easy to implement [20]. On the other hand, for the phase difference, a PI regulator is typically adopted to control the VSG output frequency, until both frequency and phase differences meet the closing standards. However, in the case of transients, significant phase jumps may appear, which inevitably affects the pre-synchronization performance, and in turn, the entire system stability.

Note that the phase is a periodic signal. For instance, as shown in Fig. 5, it varies within 0 to 2π rad during the interval of t_0 to t_1, which jumps from 2π to 0 rad at the end of the cycle at t_1, an d the next cycle starts. However, the phase jump error remains during t_1~t_2, as demonstrated in Fig. 5. It is assumed that the SG and VSG output voltage frequencies meet ω_{sg} =

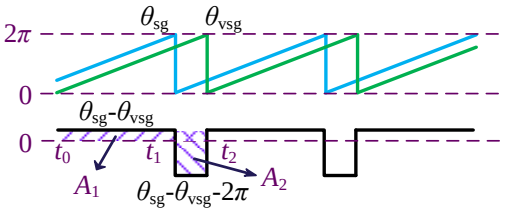

Fig. 5. Illustration of the phase jump difference.

ω_{vsg}, and the voltage phase of the SG θ_{sg} is leading that of the VSG θ_{vsg}, as illustrated in Fig. 5. Since the voltage phases of the VSG and SG units cannot be completely identical in the synchronization process, the phase will have a positive and negative jump in each cycle, which results in the continually forward and reverse adjustment of the output frequency. If the phase is directly attached to the VSG as the frequency signal $\Delta\omega$, disturbances will be induced to the VSG active loop.

Ignoring the integral unit, according to Figs. 4 and 5, the phase adjustment degree can be expressed as

$$\begin{aligned}\Delta\theta=&\int_{t_0}^{t_1}\left[\omega_{vsg}-\omega_{sg}+k_{pp}(\theta_{sg}-\theta_{vsg})\right]dt+\\&\int_{t_1}^{t_2}\left[\omega_{vsg}-\omega_{sg}+k_{pp}(\theta_{sg}-\theta_{vsg}-2\pi)\right]dt\\&=k_{pp}\left[\int_{t_0}^{t_2}(\theta_{sg}-\theta_{vsg})dt-2\pi(t_2-t_1)\right]=k_{pp}(A_1-A_2)\end{aligned}\tag{2}$$

where k_{pp} is the proportional coefficient of the phase regulator, A_1 and A_2 are shown in Fig. 5. It can be seen in (2) that when $A_1>A_2$, the phase synchronization can be achieved within longer adjustment time. When $A_1 = A_2$, the phase difference remains unchanged, and the phase synchronization cannot be achieved. When $A_1<A_2$, the VSG output phase lags more until it is equal to the last cycle of the SG output phase. As a result, the pre-synchronization time is prolonged and even the system will fail to synchronize. Moreover, when the parallel pre-synchronization is completed and SW_2 opens (see Fig. 4), the removal of the integral unit will also affect the frequency stability of the microgrid. In all, with the above analysis, the pre-synchronization should be improved in order to ensure the stability of the microgrid with parallel SG and VSG units.

B. Novel Phase Synchronization Method

Accordingly, a novel pre-synchronization method is proposed to eliminate the impact of the phase angle jump. Considering the characteristics of sine and cosine functions, their values remain the same when the phase jumps between $\triangle\theta$ and $\triangle\theta - 2\pi$. The cosine function is adopted accordingly due to its monotonicity and continuity in the range of [0, π] rad. In Fig. 6, the newly constructed function '$1 - \cos(\theta_{sg} - \theta_{vsg})$' is denoted by the line 'a'. Only part of the phase within 0~π rad is selected. Due to the non-negativity of the above constructed signal, the function '$\cos(\theta_{sg} - \theta_{vsg}) - 1$' is selected as part of the SG lagging phase (shown as the line 'b' in Fig. 6). This also ensures the regulation continuity in the phase range of [–π, π] rad. When the phase difference jumps, line 'a' and line 'b' are translated into line 'c' and line 'd', respectively, with their value and change tendencies unchanged. Therefore, the translation will not affect the phase regulation continuity.

According to the constructed function, the frequency

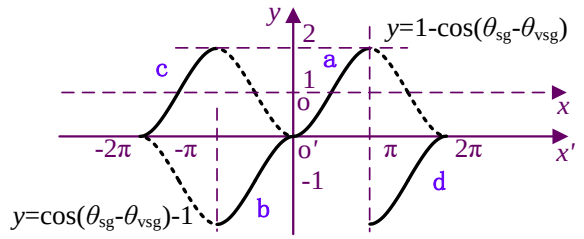

Fig. 6. Illustration of the phase transition for the novel pre-synchronization algorithm with a newly constructed function.

modulation signal can be obtained as

$$\Delta\omega=\begin{cases}k_c[1-\cos(\theta_{sg}-\theta_{vsg})], & 0<\theta_{sg}-\theta_{vsg}\le\pi\\k_c[\cos(\theta_{sg}-\theta_{vsg})-1], & -\pi<\theta_{sg}-\theta_{vsg}<0\\k_c[1-\cos(\theta_{sg}-\theta_{vsg}-2\pi)], & -2\pi<\theta_{sg}-\theta_{vsg}\le-\pi\\k_c[\cos(\theta_{sg}-\theta_{vsg}+2\pi)-1], & \pi<\theta_{sg}-\theta_{vsg}<2\pi\end{cases}\tag{3}$$

where k_c is modulation index, and the ranges of [–2π, –π] and [π, 2π] rad denote the phase difference in the of phase jumps.

With the proposed parallel pre-synchronization method in (3), the output voltage amplitude, frequency and phase of the SG and VSG units can be synchronized to avoid closing impact caused by the difference in the output voltage vector. On this basis, the transient performance of the VSG and SG parallel microgrid according to the inertia matching is then explored in the next section.

IV. Integrated Parameter Configuration Method for the VSG

A. System Inertia and Damping Parameter Matching

Taking the active power control loop in Fig. 1 as an example, the small-signal model of the VSG can be obtained according to (1) as

$$\begin{cases}J_{vsg}\omega_n s\Delta\omega_1=-\Delta P_1-D_p\Delta\omega_1\\s\Delta\delta_1=\Delta\omega_1\end{cases}\tag{4}$$

in which $\Delta\omega_1$, $\Delta\delta_1$ is the angular frequency and power angle difference, respectively, and ΔP_1 is the active power output difference of the VSG. The small-signal model of the SG speed loop is obtained as

$$J_{sg}\omega_n s\Delta\omega_2=-\Delta P_2-\frac{k_p}{1+T_d s}\Delta\omega_2\tag{5}$$

where J_{sg} is the moment of inertia from the SG, $\Delta\omega_2$ is the angular frequency difference, and ΔP_2 is the active power output difference of the SG.

Accordingly, the P-ω transfer functions of the VSG and SG active power loop can be expressed as

$$\begin{cases}G_{vsg}=\dfrac{\Delta\omega_1}{\Delta P_1}=\dfrac{1}{-J_{vsg}\omega_n s-D_p}\\G_{sg}=\dfrac{\Delta\omega_2}{\Delta P_2}=\dfrac{T_s s+1}{-J_{sg}\omega_n T_d s^2-J_{sg}\omega_n s-k_p}\end{cases}\tag{6}$$

from which it can be concluded that the SG and VSG possess the same active droop relationship, when $s\to0$, and the specific droop characteristics depend on the corresponding droop coefficient D_p and k_p, respectively. Therefore, the following damping matching relationship should be satisfied according to the system capacity [24]:

$$\begin{cases}k_p S_{sg}=D_p S_{vsg}\\k_q S_{sg}=D_q S_{vsg}\end{cases}\tag{7}$$

with S_{sg}, S_{vsg} being the capacities for the SG and VSG.

Additionally, the transient performance of the microgrid is synthetically affected by the droop coefficients, moment of inertia, and governor inertial response time constant, as shown in (6). During the transients, power oscillations, large

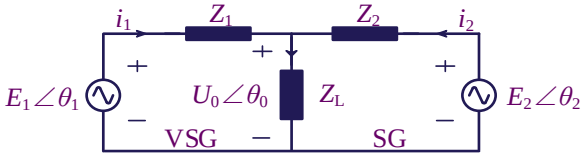

Fig. 7. Equivalent circuit diagram of the microgrid with an SG and a VSG operating in parallel.

overshoots or even system maladjustments may occur. A detailed transient analysis is required for the stability of microgrids as follows.

First, the moment of inertia [26] can be given as

$$J_{sg}=\frac{2HS}{\omega_n^2} \tag{8}$$

where H is the inertia time constant, representing the transient period (i.e., the time for the system returning to steady state), and S is the system capacity. With the flexibility of the VSG virtual inertia, the same H should be satisfied to ensure the rotor inertia matching, which is given as

$$\frac{J_{sg}}{S_{sg}}=\frac{J_{vsg}}{S_{vsg}} \tag{9}$$

After the rotor inertia and damping parameter matching are achieved, the transient regulation process and performance can be further explored based on the small-signal model.

B. Active Power Control Mode

The small-signal model of the microgrid with parallel SG and VSG units is established in this section. The VSG and SG systems are equivalent to the series connection of an ideal voltage source and output impedance at the fundamental frequency, as shown in Fig. 7. In Fig. 7, $E_1\angle\theta_1$ is the VSG output potential, $E_2\angle\theta_2$ is the SG internal potential, $U_0\angle\theta_0$ is the PCC voltage, Z_L is the load impedance, Z_1 and Z_2 are the system impedance of the VSG and SG, respectively, including the output and line impedance. According to Fig. 7, it can be obtained that:

$$U_0\angle\theta_0=\frac{\dfrac{E_1\angle\theta_1}{Z_1}+\dfrac{E_2\angle\theta_2}{Z_2}}{Z\angle\theta_z} \tag{10}$$

where $Z\angle\theta_z$ is the equivalent impedance at the PCC. Due to the inductive characteristic of the SG and virtual impedance, it is assumed that the system impedance is ideally inductive, that is, $Z_i = jX_i$ with X_i being the reactance. Here, i = 1, 2, L, represents for the VSG, SG, and load, correspondingly (see Fig. 7). The equivalent impedance can then be calculated as

$$\begin{cases} Z=\dfrac{\sqrt{\left(X_1X_2R_L\right)^2+\left[\left(X_1+X_2\right)\left(R_L^2+X_L^2\right)+X_1X_2X_L\right]^2}}{X_1X_2\left(R_L^2+X_L^2\right)} \\ \theta_z=\arctan\left[-\dfrac{\left(X_1+X_2\right)\left(R_L^2+X_L^2\right)+X_1X_2X_L}{X_1X_2X_L}\right] \end{cases} \tag{11}$$

with R_L being the load resistance.

According to the instantaneous power theory, the output active power can be expressed as

$$P_i=3\times\left[\frac{E_i^2}{Z_i}-\frac{E_i^2}{Z_i^2Z}\cos\theta_z-\frac{E_iE_j}{Z_iZ_jZ}\cos\left(\theta_z+\theta_i-\theta_j\right)\right] \tag{12}$$

where i, j are 1 and 2 for the VSG and SG, respectively. Considering the ideally inductive and uncoupled operation environment, it can be obtained that $\partial P_i/\partial E_i=\partial P_i/\partial E_j=0$. Then, due to the small impedance angle difference $\theta_i-\theta_j$, it is approximated that $\sin(\theta_i-\theta_j)=\theta_i-\theta_j$ and $\cos(\theta_i-\theta_j)=1$. Accordingly, Eq. (12) can be linearized as

$$\begin{aligned}\Delta P_i&=M\left(\Delta\theta_i-\Delta\theta_j\right)=M\left[\Delta(\theta_i-\theta_0)-\Delta(\theta_j-\theta_0)\right]\\&=M\left(\Delta\delta_i-\Delta\delta_j\right)\end{aligned} \tag{13}$$

where $M=E_iE_j\sin\theta_z/(Z_iZ_jZ)$, δ_1 and δ_2 are the output power angles of the VSG and SG, respectively.

Let $Y=[\Delta\omega_1,\Delta\omega_2]^T$, $N=[\Delta\delta_1,\Delta\delta_2]^T$ and substitute (13) into (4) and (5), and then, the state-space model of the microgrid system can be derived as

$$\dot{Y}=\begin{bmatrix}\dfrac{-D_p}{J_{vsg}\omega_n} & 0 & \dfrac{-M}{J_{vsg}\omega_n} & \dfrac{M}{J_{vsg}\omega_n}\\ 0 & \dfrac{-k_p}{J_{sg}\omega_n+J_{sg}\omega_nT_ds} & \dfrac{M}{J_{sg}\omega_n} & \dfrac{-M}{J_{sg}\omega_n}\end{bmatrix}\begin{bmatrix}Y\\N\end{bmatrix} \tag{14}$$

with Y and N being the state vectors. Eq. (14) can further be written as

$$\dot{Y}+\begin{bmatrix}\dfrac{D_p}{J_{vsg}\omega_n} & 0\\ 0 & \dfrac{k_p}{J_{sg}\omega_n(1+T_ds)}\end{bmatrix}Y=\frac{M}{\omega_n}\begin{bmatrix}\dfrac{-1}{J_{vsg}} & \dfrac{1}{J_{vsg}}\\ \dfrac{1}{J_{sg}} & \dfrac{-1}{J_{sg}}\end{bmatrix}N \tag{15}$$

which shows that when the moment of inertia and the damping are matched, the power angle couples the VSG and SG and restricts the stability of the output frequency. Moreover, the governor inertia amplifies the instability degree of the microgrid system. Considering the relationship between the output frequency and power angle shown in (4), the power angle signal can reflect the transient regulation process of the entire system. Taking the capacity ratio as $S_{vsg}/S_{sg}=n$, it can be obtained from (7) and (9) that $J_{vsg}/J_{sg}=k_p/D_p=n$, and the small signal models of the VSG and SG active loop are subtracted, which gives

$$\begin{aligned}\Delta P_2-\Delta P_1&=J_{sg}\omega_ns(n\Delta\omega_1-\Delta\omega_2)+\frac{D_p}{n}n\Delta\omega_1-\frac{k_p}{1+T_ds}\Delta\omega_2\\&=(J_{sg}\omega_ns+\frac{D_p}{n})(n\Delta\omega_1-\Delta\omega_2)-A\Delta\omega_2\end{aligned} \tag{16}$$

with $A=k_p/(1+T_ds)-D_p/n$. The droop relationship of the SG prime mover governor is expressed as $k_p\Delta\omega_2=P_{set\_sg}-P_{m\_sg}$, where P_{m_sg} is the mechanical power. Then, the transient dynamics can be expressed as

$$A\Delta\omega_2\approx\frac{k_p}{T_ds}s\Delta\delta_2-\frac{1}{n^2}(P_{set\_sg}-P_{m\_sg})=\frac{k_p}{T_d}\Delta\delta_2-\frac{\Delta P_m}{n^2}=\Delta P_{sg} \tag{17}$$

Let $\Delta P_{set\_vsg}=\pm k_{set}\Delta\delta_2$, where k_{set} is the active power setting coefficient of the VSG, ΔP_{set_vsg} and $\Delta\delta_2$ are the process variables. The VSG setting active power P_{set_vsg} must not exceed the ideal system capacity. It maintains the constant

value calculated by the capacity ratio in (7), when δ_2 keeps constant, which gives the VSG active power according to the transient regulation process. Moreover, this also compensates for the governor inertia delay of the SG to some extent. If $\Delta\delta_1$ and $\Delta\delta_2$ have the opposite signs, the active power flows within the microgrid and the negative sign is selected; if $\Delta\delta_1$ and $\Delta\delta_2$ have the same signs, the load power changes and the positive sign is selected. Then, Eq. (16) can be written as

$$(J_{sg}\omega_n s+\frac{D_p}{n})(n\Delta\omega_1-\Delta\omega_2)=\Delta(P_2+P_{sg}-P_1-P_{set\_vsg}) \\ =\Delta(P_2'-P_1)\mp k_{set}\Delta\delta_2 \quad (18)$$

By selecting different active power setting coefficient, i.e., k_{set}, the governor inertia matching between the VSG and SG is realized to ensure the transient stability during transient cases. The transient performance of the reactive power loop depends on the excitation regulation mode and the power decoupling degree of the system, and the similar ideas can also be applied in the reactive power regulation of the VSG and SG.

C. Parameter Design

Take $\Delta\omega = n\Delta\omega_1 - \Delta\omega_2$ and $\Delta\delta = n\Delta\delta_1 - \Delta\delta_2$ as new state variables. Because $\Delta\delta_2$ is much larger than $\Delta\delta_1$, the small-signal model of the microgrid system can be simplified as

$$(J_{sg}\omega_n s+\frac{D_p}{n})\Delta\omega+2M\Delta\delta=2M(n-1)\Delta\delta_1-k_{set}\Delta\delta_2 \\ \approx -k_{set}\Delta\delta \quad (19)$$

Then, the characteristic equation of the system is obtained as

$$G(s)=s^2+\frac{D_p}{J_{sg}\omega_n n}s+\frac{2M+k_{set}}{J_{sg}\omega_n} \quad (20)$$

According to the Routh criteria, when $2M+k_{set}>0$, the system has no characteristic roots with positive real parts and the system is stable. However, for $\sin\theta_z<0$, it is more usual in the inductive operational condition, and the necessity of the proposed power setting method is obvious.

It is assumed that the system keeps stable, and the damping ratio is calculated as

$$\zeta=\frac{D_p}{2n}\sqrt{\frac{Z_1Z_2Z}{J_{sg}\omega_n(2E_1E_2\sin\theta_z+k_{set}Z_1Z_2Z)}} \quad (21)$$

indicating that the damping ratio is related to k_{set} under invariant D_p and J_{sg}, which is set as 0.6~0.8 for the optimum performance. In order to simplify the analysis, Z_1Z_2Z is set as 5, $\sin\theta_z$ is set as – 0.1, the capacity ratio n is set as 1 and k_{set} is set as 210, 260 and 310, respectively. The poles of the closed-loop system are then shown in Fig. 8.

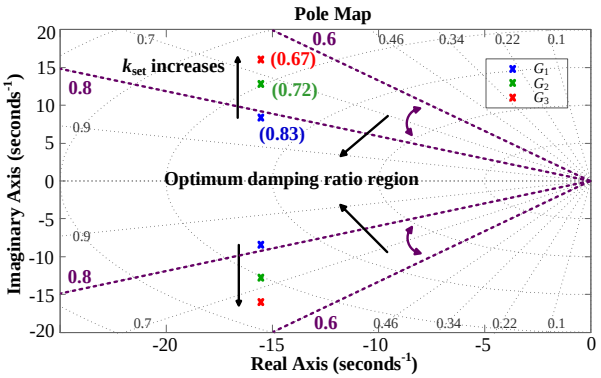

Fig. 8. Pole map of the closed-loop system of the microgrid.

It can be observed in Fig. 8 that the characteristic roots of the three cases (i.e., k_{set} = 210, 260 and 310) have the same distance to the imaginary axis. This means that the setting coefficient k_{set} does not affect the stability of the entire system. The poles of G_1 (k_{set} = 210) is outside the optimum damping ratio region. With the increase of k_{set}, the distance between the characteristic roots and real axis becomes larger. As a result, the damping of the system with G_3 (k_{set} = 310) is smaller than that of the system with G_2 (k_{set} = 260), which is easy to oscillate but with short regulating time. Keeping increasing k_{set} will move the poles out of the optimum damping ratio region and the stability will become worse. Therefore, the compromise is to consider the overshoot and regulating time to calculate the setting coefficient k_{set}.

V. Simulation Results

A. Simulation Model Description and Test

To verify the proposed pre-synchronization method and the active power setting mode, simulations are carried out on a microgrid with SG and VSG units in MATLAB/Simulink. Various cases are considered and the parameters of the system are shown in Table I.

Firstly, when the amplitude and frequency of the SG and VSG output voltages have been synchronized, the phase difference keeps as a constant and jumps once per cycle without the phase synchronization, as shown in Fig. 9. The phase difference cannot meet the precision requirement of closing, and this has been analyzed in Section III.A. Then, the

TABLE I
Parameters of the Microgrid System.

Parameter	Value
Moment of inertia, Virtual inertia (J_{sg}, J_{vsg})	0.0923 kg·m^2
System capacity of SG and VSG (S_{sg}, S_{vsg})	8000 VA
Stator impedance (R_{s_sg}, L_{s_sg})	1.62 Ω, 4.5 mH
Rated electromotive force (E_0)	220 V
Rated rotor speed (n_0)	1500 rpm
GOV, AVR droop coefficient (k_p, k_q)	900, 320
AVR PI coefficient (k_{p_AVR}, k_{i_AVR})	30, 100
Inertial response time constant (T_d)	0.5 s
Rated voltage amplitude (U_n)	220 V
Rated angular frequency (ω_n)	314.1 rad/s
P-f, Q-V Droop coefficient (D_p, D_q)	900, 320
VSG voltage coefficient (K)	6.5
Virtual impedance (R_v, L_v)	0.08 Ω, 8 mH
Coefficient of the frequency regulator (K_1)	3000
Coefficients of the phase regulator (k_{pp}, k_{ip})	3.5, 1.75
Pre-synchronization modulation index (k_c)	30
DC voltage (V_{in})	600 V
VSG switching frequency (f_n)	10 kHz
Line impedance (Z_{line})	(0.308+j0.47) Ω/km
LC filter (L, C)	3.08 Ω, 3.2 mH, 1.2 mF

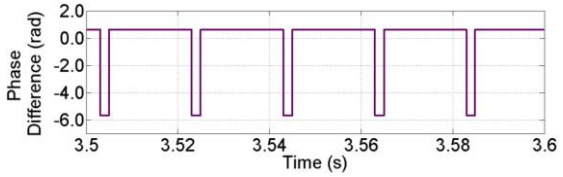

Fig. 9. Phase difference jump.

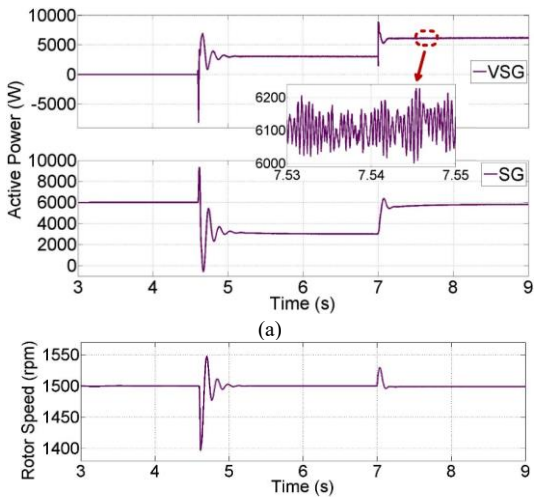

Fig. 10. Simulation results of the microgrid model performance test: (a) the output active power and (b) the SG rotor speed.

operation performance and load performance of the parallel model without the proposed methods are then studied. In this case, a traditional PI frequency method (see Fig. 4) is used and the VSG is cut in at t = 4.6 s sharing 6-kW load with the SG. At t = 7 s, another 6-kW load is cut in. The simulation results of the system in response to cutting-in operation are presented in Fig. 10. From the results, it is known that the instantaneous closing power affects the system performance due to the poor pre-synchronization accuracy. In addition, the power allocation basically meets the requirements under the premise of the matched parameters as discussed in Section IV. However, the adjusting inertia difference causes the SG rotor speed to abnormally rise, and then, the power and frequency oscillations at a high frequency occur in the microgrid, as also described in [16]. The oscillation amplitude is almost 200 W, which affects the operation of any other electrical equipment.

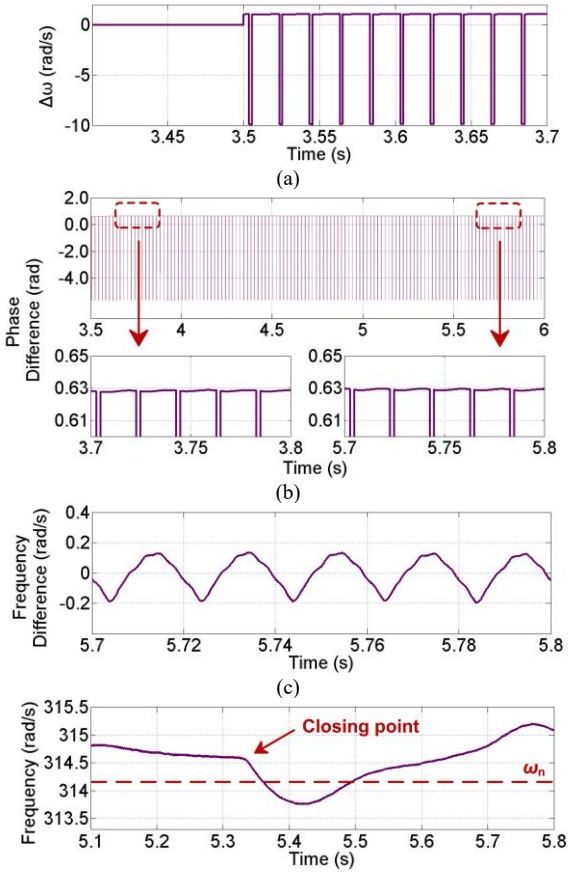

Fig. 11. Simulation results of the microgrid with the traditional pre-synchronization method: (a) frequency modulation signal, (b) phase difference, (c) frequency difference, and (d) VSG output frequency.

B. Parallel Pre-synchronization

In this section, the performances of the microgrid with the traditional pre-synchronization method (i.e., using a PI regulator for the phase synchronization) [20] and the proposed pre-synchronization method are compared to verify the effectiveness of the proposed solution. Specifically, before t = 3.5 s, the SG is operating solely with a 6-kW load. At t = 3.5 s, the VSG is cut in and it is operating in the pre-synchronization mode.

The simulation results of the microgrid with the traditional pre-synchronization method are presented in Fig. 11. In this case, a PI regulator is applied in the phase synchronization, in which k_{pp} and k_{ip} are the proportional and integral coefficients, respectively (see Fig. 4). As observed in Fig. 11(a), there is a negative jump per cycle in the frequency modulation signal $\Delta\omega$

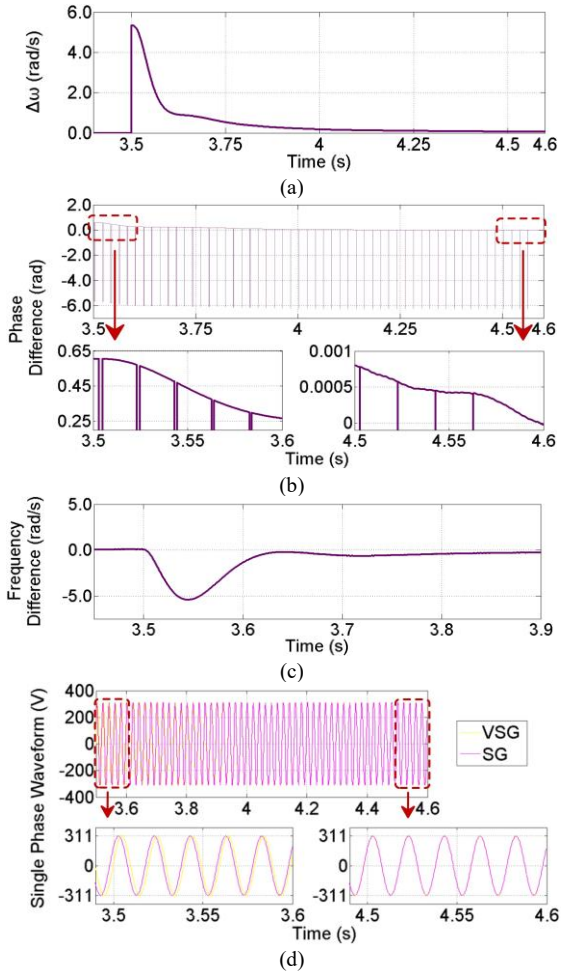

Fig. 12. Simulation results of the microgrid with the proposed parallel pre-synchronization method: (a) frequency modulated signal, (b) phase difference, (c) frequency difference, and (d) synchronization process of single phase.

due to the proportional unit. For the phase difference, it can be seen in Fig. 11(b) that the phase difference slightly increases from t = 5.8 s, corresponding to the condition that $S_1 \leq S_2$, which causes the phase difference to remain almost unchanged, and thus the system fails to synchronize. Meanwhile, the frequency difference is also unstable with oscillations, as demonstrated in Fig. 11(c). Additionally, supposing that the output phase can be synchronized, the removal of the integral unit results in a sudden drop of the VSG frequency, as shown in Fig. 11(d). This will affect the transient performance of the system during closing, as discussed in the previous sections.

However, with the proposed pre-synchronization method, better performances can be achieved, as verified in Fig. 12. In this case, the closing standard [17] is met at t = 4.58 s. As indicated in Fig. 12(a), the frequency modulation signal is continuous and monotonous, and keeps smooth in the case of the phase difference jump. The phase and frequency differences are shown in Fig. 12(b) and (c), respectively. It can be observed that the difference can be adjusted smoothly and quickly to zero, avoiding the drop issue in the case of the conventional method, as shown in Fig. 11(d). In all, the proposed method satisfies the requirements for the synchronization. Moreover, Fig. 12(d) shows the synchronization process of phase A of the VSG and SG output voltages. Rapidity and smoothness of synchronization regulation are intuitively reflected in Fig. 12(d). With the proposed pre-synchronization method, further simulations about the transient performance of the VSG and SG units during transient cases are carried out in the next section.

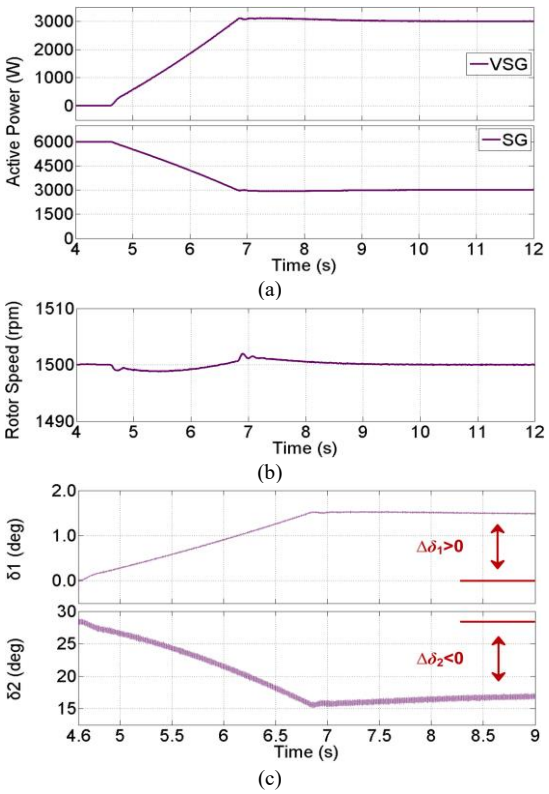

Fig. 13. Simulation results of the microgrid with the power setting mode control under a closing transition: (a) output active power, (b) SG rotor speed, and (c) power angle.

C. Closing and Loading Transition

1) Performance under Closing Transition

In this simulation, the capacity ratio of the VSG and SG is set as 1:1 and taking n = 1 to calculate the active power setting coefficient k_{set}, which is convenient to verify the ability of the steady power sharing that is not affected by the proposed transient algorithm. From the above section, the VSG is cut in at t = 4.58 s and the transient closing impact caused by the poor parallel pre-synchronization is eliminated. As it can be observed in Fig. 13, the transient performance under the closing transition is improved when the new parallel pre-synchronization method and the active power setting mode are adopted. Here, k_{set} is calculated as 265. The transition time is prolonged according to the governor inertia delay of the SG, which suppresses the transient oscillation in the SG rotor speed and smooths the power transition. Moreover, $\Delta\delta_1$ and $\Delta\delta_2$ have the opposite signs in this case and $-k_{set}\Delta\delta_2$ is selected as ΔP_{set_vsg} to adjust the active power setting for the VSG. In all, the simulation is in agreement with the discussion and the analysis in Section IV.B, meaning that the proposed methods are verified.

2) Performance under Loading Transition

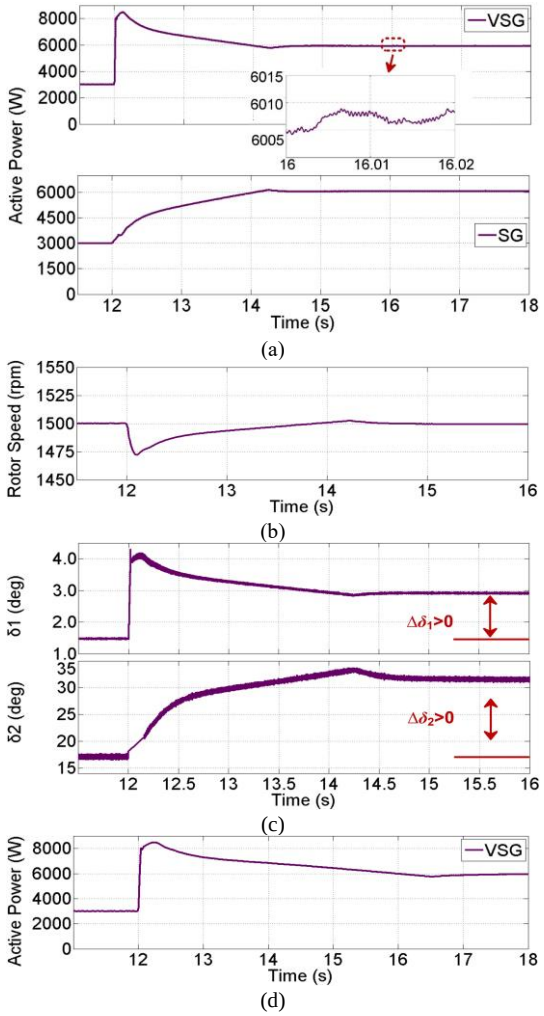

Fig. 14. Simulation results of the microgrid with the power setting mode under a loading transition: (a) output active power, (b) SG rotor speed, (c) power angle, and (d) output active power with a smaller k_{set}.

In this case, a 6-kW resistive load is suddenly added in the system at t = 12 s and the results are shown in Fig. 14 with k_{set} being unchanged. As observed in Fig. 14(a), the prime mover of the SG responds slowly to the loading requirement, while the VSG is compensating for part of the power vacancy and matches the governor inertia of the SG smoothly. The amplitude of high frequency power oscillation decreases greatly to acceptable level. Seen from Fig. 14(b), the SG rotor speed drops a little normally and recovers to the rated value with no transient oscillations within 3 s. Additionally, $\Delta\delta_1$ and $\Delta\delta_2$ have the same sign and $k_{set}\Delta\delta_2$ is selected as ΔP_{set_vsg} in this case, which also agrees with the analysis in Section IV.B. Fig. 14(d) further shows the simulation result of the VSG output power with k_{set} being 220. Compared with the results in Fig. 14(b), it is known that both cases can reach the power limiting, but the system with smaller k_{set} operates with longer regulation time, as shown in Fig. 14(d). As a result, dynamics should be considered first when calculating k_{set} in the optimum damping ratio region, since the power limiting plays an important role in maintaining the stability. In all, the above case studies by simulations verify the correctness and effectiveness of the proposed control methods.

VI. Conclusion

In this paper, microgrids consisting of SG and VSG units in parallel were explored, and the control and coordination of generation resources under different inertia were discussed. It has been revealed that the system stability is challenged depending on the inherent differences between the SG and VSG, especially in the case of transients. Accordingly, a new pre-synchronization control method and a novel active power setting mode for the VSG were proposed to improve the transient performance of the microgrid. Simulation results have demonstrated that oscillations in the active power loop are effectively eliminated with the proposed methods. In addition, it should be pointed out that the methods are also beneficial to other grid-connected systems to eliminate the phase errors, and the control studies of compatibly interconnecting different power supplies.

References

[1] H. Bevrani, T. Ise, and Y. Miura, "Virtual synchronous generators: a survey and new perspectives," *International Journal of Electrical Power & Energy Systems*, vol. 54, no. 1, pp. 244-254, Jan. 2014.

[2] D. Li, Q. Zhu, and S. Lin, "A self-adaptive inertia and damping combination control of VSG to support frequency stability," *IEEE Transactions on Energy Conversion*, vol. 32, pp. 397-398, Mar. 2017.

[3] J. Liu, D. Yang, W. Yao, R. Fang, H. Zhao, and B. Wang, "PV-based virtual synchronous generator with variable inertia to enhance power system transient stability utilizing the energy storage system," *Protection and Control of Modern Power Systems*, vol. 2, no. 2, pp. 429-437, Dec. 2017.

[4] Y. Cao, W. Wang, and Y. Li, "A virtual synchronous generator control strategy for VSC-MTDC systems," *IEEE Transactions on Energy Conversion*, vol. 33, no. 2, pp. 750-761, Jun. 2018.

[5] B. Li and L. Zhou, "Power decoupling method based on the diagonal compensating matrix for VSG-controlled parallel inverters in the microgrid," *Energies*, vol. 10, no.12, pp. 1-13, Dec. 2017.

[6] K. Shi, G. Zhou, and P. Xu, "The integrated switching control Strategy for grid-connected and islanding operation of micro-grid inverters based on a virtual synchronous generator," *Energies*, vol. 11, no. 6, pp. 1544, Jun. 2018.

[7] Y. Ma, W. Cao, L. Yang, F. Wang, and L.M. Tolbert, "Virtual synchronous generator control of full converter wind turbines with short term energy storage," *IEEE Transactions on Industrial Electronics*, vol. 64, no. 11, pp. 8821-8831, Apr. 2017.

[8] S. Haider, G. Li, and K. Wang, "A dual control strategy for power sharing improvement in islanded mode of AC microgrid," *Protection and Control of Modern Power Systems*, vol. 3, no. 1, Dec. 2018.

[9] J. Liu, Y. Miura, and T. Ise, "Enhanced virtual synchronous generator control for parallel inverters in microgrids," *IEEE Transactions on Smart Grid*, vol. 8, no. 5, pp. 2268-2277, Sep. 2017.

[10] H. Xu, X. Zhang, and F. Liu, "A reactive power sharing strategy of VSG based on virtual capacitor algorithm," *IEEE Transactions on Industrial Electronics*, vol. 64, no. 9, pp. 7520-7531, Mar. 2017.

[11] B. Zhang, X. Yan, Y. Huang, Z. Liu, and X. Xiao, "Stability control and inertia matching method of multi-parallel virtual synchronous generators," *Transactions of China Electrotechnical Society*, vol. 32, no. 10, pp. 42-52, May. 2017. (in Chinese)

[12] Q. Song, H. Zhang, K. Sun, and Y. Wei, "Improved adaptive control of inertia for virtual synchronous generators in islanding micro-grid with multiple distributed generation units," *Proceedings of the CSEE*, vol. 37, no. 2, pp. 412-424, Feb. 2017. (in Chinese)

[13] A. D. Paquette, M. J. Reno, R. G. Harley, and D. M. Divan, "Sharing transient loads: causes of unequal transient load sharing in islanded microgrid operation," *IEEE Industry Applications Magazine*, vol. 20, no. 2, pp. 23-34, Mar. 2014.

[14] Y. Banjo, Y. Miura, and T. Ise, "Enhanced stand-alone operating characteristics of an engine generator interconnected through the inverter using virtual synchronous generator control," in *Proc. of International Conference on Power Electronics & Ecce Asia*, 2015, DOI: 10.1109/ICPE.2015.7167904.

[15] K. Sakimoto, Y. Miura, and T. Ise, "Characteristics of parallel operation of inverter-type distributed generators operated by a virtual synchronous generator," *Electrical Engineering in Japan*, vol. 192, no. 4, pp. 9-19, Sep. 2015.

[16] J. Liu, M. Yushi, T. Ise, J. Yoshizawa, and K. Watanabe, "Parallel operation of a synchronous generator and a virtual synchronous generator under unbalanced loading condition in microgrids," in *Proc. of Power Electronics and Motion Control Conference*, 2016, DOI: 10.1109/IPEMC.2016.7512894.

[17] K. Shi, W. Song, P. Xu, R. Liu, Z. Fang, and J. Yi, "Low-voltage ride-through control strategy for a virtual synchronous generator based on smooth switching," *IEEE Access*, vol. 6, pp. 2703-2711, Dec. 2017.

[18] Q. Zhong, P. Nguyen, and Z. Ma, and W. Sheng, "Self-synchronized synchronverters: inverters without a dedicated synchronization unit," *IEEE Transactions on Power Electronics*, vol. 29, no. 2, pp. 617-630, Feb. 2014.

[19] Y. Wei, H. Zhang, and K. Sun, "Pre-synchronization method of virtual synchronous generator using virtual power," *Automation of Electric Power Systems*, vol. 40, no. 12, pp. 124-129, Dec. 2016.

[20] J. Liu, M. J. Hossain, J. Lu, F.H.M. Rafi, and H. Li, "A hybrid AC/DC microgrid control system based on a virtual synchronous generator for smooth transient performances," *Electric Power Systems Research*, vol. 162, pp. 169-182, Sep. 2018.

[21] R. Imran and S. Wang, "Enhanced two-stage hierarchical control for a dual mode WECS-based microgrid," *Energies*, vol. 11, no. 5, pp. 1270, May. 2018.

[22] T. Shintai, Y. Miura, and T. Ise, "Oscillation damping of a distributed generator using a virtual synchronous generator," *IEEE Transactions on Power Delivery*, vol. 29, no. 2, pp. 668-676, Mar. 2014.

[23] X. Wang, Y. Li, and F. Blaabjerg, "Virtual-impedance-based control for voltage-source and current-source converters," *IEEE Transactions on Power Electronics*, vol. 30, no. 12, pp. 7019-7037, Dec. 2015.

[24] Q. Zhong and G. Weiss, "Synchronverters: inverters that mimic synchronous generators," *IEEE Transactions on Industrial Electronics*, vol. 58, no. 4, pp. 1259-1267, Apr. 2011.

[25] G. Jin, L. Li, G. Li, and Z. Wang, "Accurate proportional load sharing among paralleled inverters based on improved P-V droop coefficient," *Electric Power System Research*, vol. 143, pp. 312-320, Feb. 2017.

[26] J. Alipoor, Y. Miura, and T. Ise, "Stability assessment and optimization methods for microgrid with multiple VSG units," *IEEE Transactions on Smart Grid*, vol. 9, no. 2, pp. 1462-1471, Mar. 2018.